Molecular mobility in piezoelectric hybrid nanocomposites with 0-3 connectivity: Particles size influence

Jean-Fabien Capsal, Eric Dantras *, Jany Dandurand, Colette Lacabanne

Laboratoire de Physique des Polymères, Institut CARNOT - CIRIMAT Université Paul Sabatier, 31062 Toulouse, France

Keywords:
Dynamic dielectric spectroscopy;
Thermostimulated currents;
Hybrid nanocomposites;
Molecular mobility

A B S T R A C T

Polyamide 11/barium titanate nanocomposites have been studied by a combination of dynamic dielectric spectroscopy, thermo stimulated current and differential scanning calorimetry. The correlation between results obtained by dielectric and calorimetric methods allows us to describe the evolution of the physical structure of the hybrid nanocomposites. The molecular mobility of 0-3 connectivity nanocomposites has been explored. The influence of the nanoparticles size is specifically studied. The smaller sized fillers produce a shift of the relaxation modes observed above the glass transition temperature of polyamide 11 towards lower frequency. The increase of the organic/inorganic interface induces an increase of the ratio rigid amorphous phase/soft amorphous phase. The interfaces favour local ordering stabilized by hydrogen bonds at a nanometric scale.

1. Introduction

Since the discovery of the ferroelectric behaviour of some class of polymers [1–6], these materials have attracted a great interest due to their good piezo/pyroelectric properties, low permittivity, lightweight and ductility [7]. These materials have potential use as sensors and electromechanical transductors. However, the poling field required to give a ferroelectric property to these materials is high [8–10] that could restrict their use in some particular cases. Ferroelectric ceramics such as barium titanate are commonly used for their high electroactive properties and low poling field [11,12]. In order to overcome the disadvantage of high poling field of organic ferroelectrics, inorganic particles are dispersed into a polymeric matrix to realize a 0-3 connectivity according to the Newnham nomenclature [13]. Previous works have shown that the piezo/pyroelectric properties of these composites have a poling field more than 20 times lower than ferroelectric polymers [14–17]. The final electroactive properties of these composites are close to the ones of organic materials while keeping the ductility of the polymeric matrix [18].

Few works have been devoted to the influence of the inorganic phase on the physical structure of the organic amorphous phase. In this study we report the particles size influence of inorganic ferroelectric barium titanate on the molecular dynamics of the polyamide 11 amorphous phase. Broadband dynamic dielectric spectroscopy and thermo stimulated current experiments have been combined to explore the physical structure of these composites at a nanometric scale in a broad frequency range.

* Corresponding author.
E-mail address: dantras@cict.fr (E. Dantras).

doi:10.1016/j.jnoncrysol.2010.06.037

2. Experimental

2.1. 0-3 hybrid nanocomposites elaboration

The mean diameter of barium titanate nanoparticles is ranging from 50 nm to 700 nm. Polyamide 11 (PA 11) powder was dissolved in a solution of dimethyl acethyl amide (DMAc) and the required barium titanate ($BaTiO_3$) powder was dispersed to form a mixture by ultrasonic stirring. The samples were dried over night at 110 °C to remove the solvent. The hybrid nanocomposites were hot pressed to form thin films from 100 to 150 μm thick. In order to conserve the same connectivity of the inorganic particles into the polymeric matrix, the volume fraction of $BaTiO_3$ has been fixed at 12 vol.%.

The experimental protocol of dispersion of barium titanate in the polymeric matrix has been checked by scanning electron microscopy (SEM). Fig. 1 shows cryo-cut samples of PA 11/$BaTiO_3$ nanocomposites for $\phi = 12$ vol.% with particles size ranging from 50 nm to 700 nm. A homogeneous dispersion at nanometric scale is observed. In the specific case of composites elaborated with 50 nm particles, 1 μm aggregates are observed. For $\phi = 24$ vol.%, an important agglomeration is observed with 100 nm $BaTiO_3$ particles but none with 300 nm. It appears that the limit particles size to compare composites in the same connectivity is 50 nm for $\phi = 12$ vol.% and 300 nm for a volume fraction of 24 vol.%.

2.2. Differential scanning calorimetry measurements

Standard differential scanning calorimetry (DSC) measurements were performed using a DSC/TMDSC 2920 set up. The sample temperature was calibrated using the onset of melting of tin (Tm = 231.88 °C), indium (Tm = 156.6 °C) and cyclohexane (Tm = 6 °C) with a heating rate of

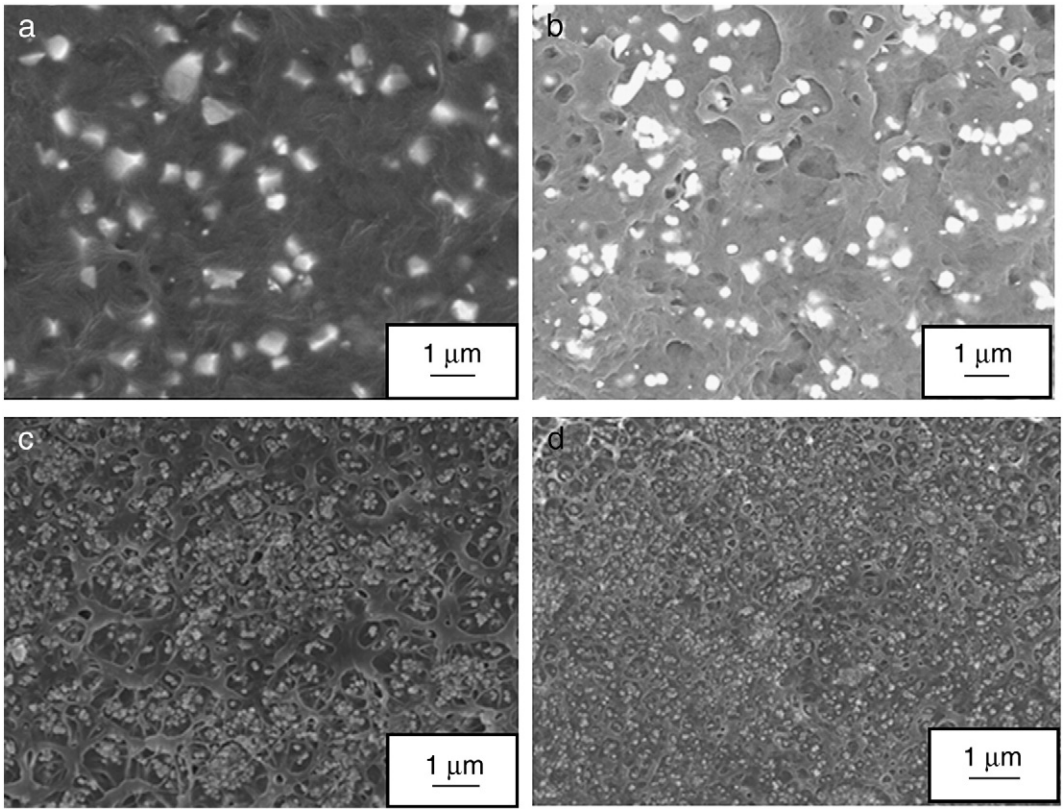

Fig. 1. Scanning electron microscope (SEM) images of PA 11/$BaTiO_3$ composites with $\phi = 12\%$ and particles size of (a) 700 nm, (b) 300 nm, (c) 100 nm and (d) 50 nm.

$q_h = +5\ °C\ min^{-1}$. The heat-flow was calibrated with the heat melting of indium ($\Delta H = 28.45\ J\ g^{-1}$); its baseline was corrected with sapphire. DSC experiments were systematically carried out over a temperature range from the equilibrium state (in order to remove the effect of previous thermal history) $T_{eq} = T_m + 20\ °C$ down to the glassy state $T_0 = Tg - 20\ °C$ with a constant cooling rate $q_c = +10\ °C\ min^{-1}$. The temperature T_0 was maintained constant for 1 h. This thermal history allows us to get a better definition of T_g usually difficult to observe on polyamide. For each sample, the glass transition temperature and the specific heat capacity step were measured by Standard DSC during a heating scan ($q_h = +10\ °C\ min^{-1}$).

2.3. Non isothermal and isothermal dielectric measurements

Thermo stimulated currents (TSC) were recorded on a TSC/RMA Analyser. For complex thermograms, the sample was polarized by an electrostatic field during $t_p = 2$ min over a temperature range from the polarization temperature $T_p = 80\ °C$ down to the freezing temperature $T_0 = 0\ °C$. Then, the field was turned off and the depolarization current was recorded with a constant heating rate $q_h = +7\ °C\ min^{-1}$; the equivalent frequency of the TSC thermograms was $f_{eq} \sim 10^{-2} - 10^{-3}$ Hz. Elementary TSC thermograms were performed with a poling window of 5 °C. Then the field was removed and the sample cooled down to a temperature $T_{cc} = T_p - 30\ °C$. The depolarization current was recorded with a constant heating rate q_h. Series of elementary thermograms were recorded by shifting the poling window by 5 °C towards higher temperature. Prior to any experiment, the samples were dehydrated during 30 min at 140 °C.

Dynamic dielectric spectroscopy (DDS) experiments were performed using a BDS 400 spectrometer covering a frequency range of 10^{-2} Hz − 3.10^6 Hz with 10 points per decade. The samples were 3 cm in diameter and prior to any measurement the composites have been also dehydrated for 4 h at 140 °C. Experiments were carried out in a temperature range from −150 °C to 150 °C. Dielectric isothermal spectra were measured every 2 °C. Before each frequency scan, temperature was kept constant to ±0.2 °C. The real ε′ and imaginary ε″ parts of the relative complex permittivity ε_T^* were recorded as a function of frequency F at a given temperature T.

The dielectric loss modulus M″ is deduced from the real and the imaginary part of the dielectric permittivity ε′ and ε″, according to Eq. 1:

$$M'' = \varepsilon'' / \left(\varepsilon'^2 + \varepsilon''^2\right) \quad (1)$$

In the modulus formalism, Maxwell–Wagner–Sillars (MWS) polarization which usually occurs in heterogeneous systems like semi-crystalline polymers [19,20] is observed as a mode. In the ε″ formalism, the MWS peak is sometimes hidden by the conductivity tail. Furthermore, a simple ohmic conductivity contribution in the loss part of the complex dielectric function results in a peak in the loss part of the modulus.

3. Results

In this section, the particles size influence of $BaTiO_3$ nanoparticles on the molecular mobility of the PA11 amorphous phase is shown by means of dielectric techniques. The particles size is ranging from 50 nm to 700 nm.

3.1. Dielectric relaxation modes in dynamic spectroscopy

The influence of the filler size on the relaxation dynamics of PA 11/$BaTiO_3$ nanocomposites was characterized by DDS. As the connectivity of composites governs the final mechanical and electric properties [13], the choice of the volume fraction is crucial. Since we have observed that nanoparticles tend to aggregate for the highest $BaTiO_3$ contents, the volume fraction is maintained at 12%.

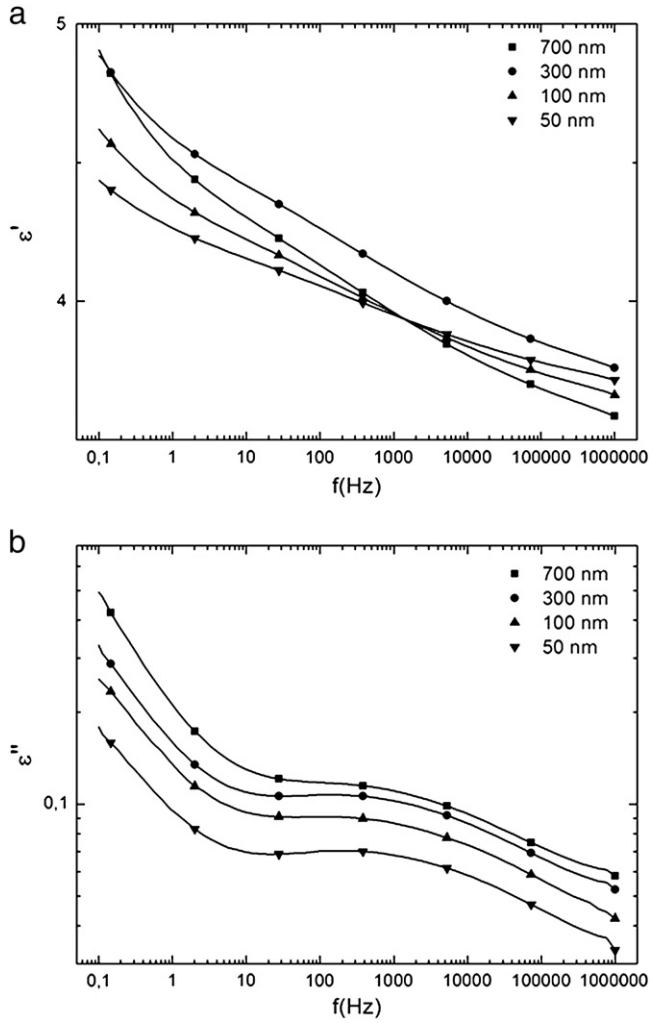

Fig. 2. Frequency dependence of (a) ε′ and (b) ε″ (T = 26 °C) of PA 11/ $BaTiO_3$ composites with ϕ = 12% and particles size of (■) 700 nm, (●) 300 nm, (▲) 100 nm and (▼) 50 nm.

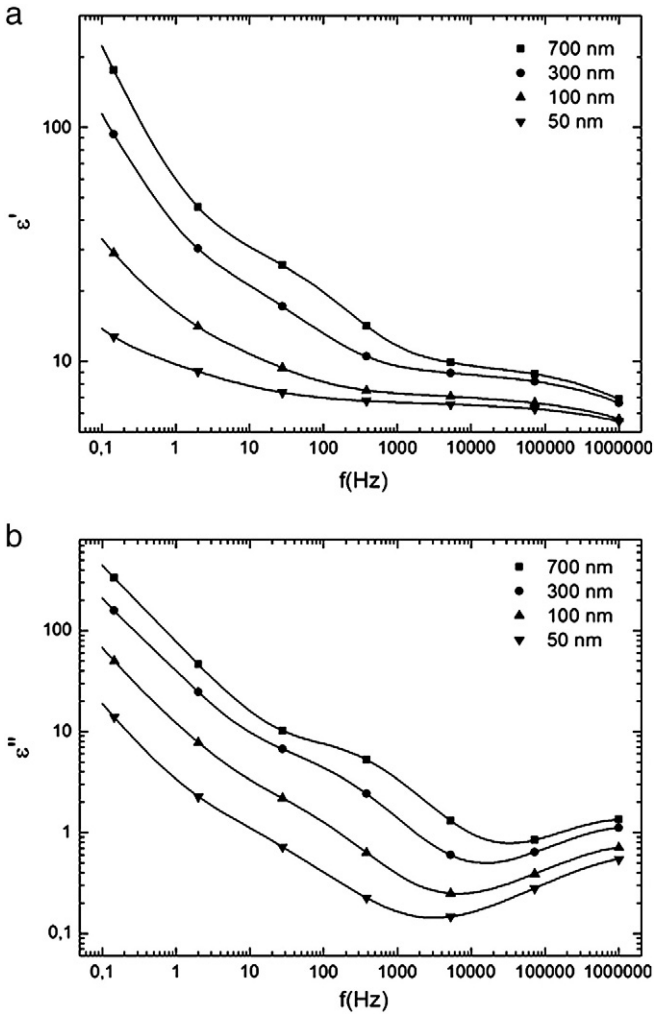

Fig. 4. Frequency dependence of (a) ε′ and (b) ε″ (T = 100 °C) of PA 11/$BaTiO_3$ composites with ϕ = 12% and particles size of (■) 700 nm, (●) 300 nm, (▲) 100 nm and (▼) 50 nm.

Dielectric permittivity at room temperature is plotted as function of frequency in Fig. 2a. The real part of ε^* is equal to ε′ = 4 at 1 kHz. At ϕ = 12%, the particles size has a weak influence on ε′. Fig. 2b reports the decrease of ε″ with the particles size. The β relaxation mode of the polyamide is pointed out; the front in the low frequency tail is associated with the dielectric manifestation of the glass transition; i.e. the α mode which appears at higher temperature.

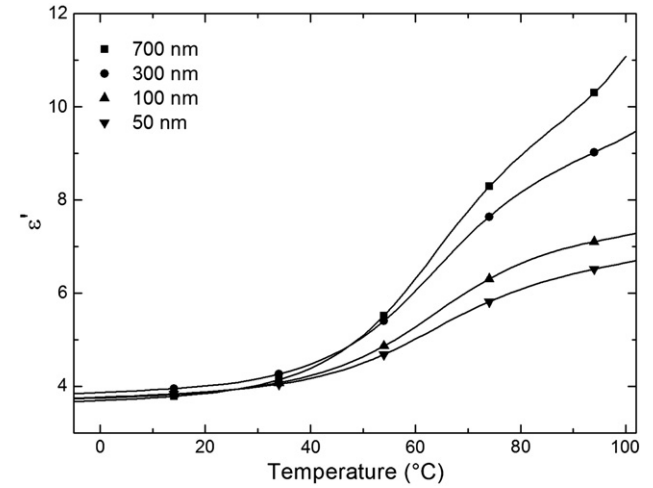

Fig. 3. Temperature evolution of ε′ (f = 1 kHz) of PA 11/$BaTiO_3$ composites with ϕ = 12% and particles size of (■) 700 nm, (●) 300 nm, (▲) 100 nm and (▼) 50 nm.

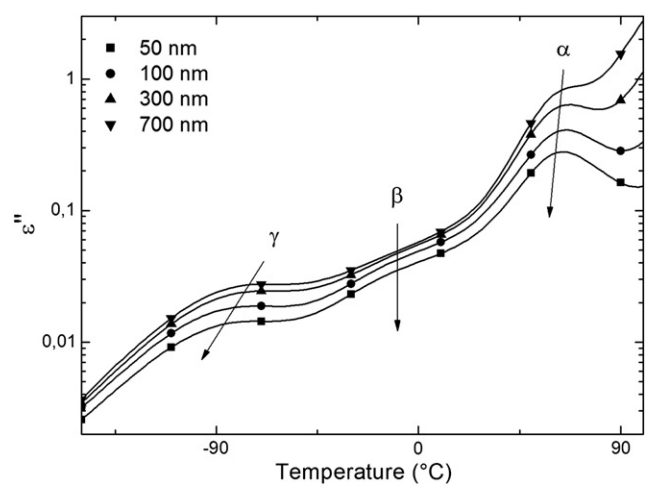

Fig. 5. Temperature dependence of ε″ (f = 1 kHz) of PA 11/$BaTiO_3$ composites with ϕ = 12% and particles size of (▼) 700 nm, (▲) 300 nm, (●) 100 nm and (■) 50 nm.

Table 1
Arrhenius parameters of γ relaxation and VTF parameters of α relaxation of PA11/ $BaTiO_3$ composites with $\phi = 12\%$ and particles size of 700 nm, 300 nm, 100 nm and 50 nm.

Size (nm)	Mode γ τ_0 (s)	Mode γ E_a (kJ/mol)	Mode α τ_0 (s)	Mode α τ_f (K^{-1})	Mode α T_0 (K ± 10 K)	Mode α $D = 1/\alpha T_0$
700 nm	4×10^{-17}	46 ± 1	6×10^{-12}	1×10^{-3}	275	3.5
300 nm	1×10^{-16}	42 ± 1	1×10^{-13}	6×10^{-4}	246	7
100 nm	5×10^{-16}	40 ± 1	4×10^{-20}	1×10^{-4}	157	39
50 nm	6×10^{-16}	39 ± 1	6×10^{-17}	3×10^{-4}	206	17

The evolution versus temperature of ε′ at 1 kHz for PA11/$BaTiO_3$ is reported in Fig. 3. These thermograms clearly show that the particles size does not affect ε′ at low frequency. In the temperature range from 60 °C to 80 °C, a step of ε′ is pointed out; it has been attributed to the dielectric manifestation of the glass transition. The dielectric strength Δε associated with the α relaxation mode decreases with the particles size. For the composite elaborated with 700 nm particles Δε is equal to 7.3 and it is divided by two with 100 nm particles. The decrease of Δε indicates that the high temperature and low frequency dielectric behaviour is more sensitive to particles size.

On the high temperature side, a front is observed for 700 nm and 300 nm composites and it disappears for lower particles size. It has been associated with the Maxwell–Wagner–Sillars (MWS) polarization due to heterogeneities.

Fig. 4a and b reports the evolution of the real and imaginary parts of the dielectric permittivity measured at 100 °C. Three dielectric contributions have been observed: the dielectric manifestation of the glass transition α, the response of the constrained amorphous phase α′ and the MWS depolarization. For this isotherm, the MWS phenomenon decreases slightly with the particles size. The dielectric permittivity at 0.1 Hz with 300 nm $BaTiO_3$ is 10 times higher than for the 100 nm composites.

The variation of ε″ versus temperature is shown in Fig. 5 for the different particles sizes. Three relaxation modes are clearly identified: a lower temperature mode γ at −90 °C associated with the relaxation of aliphatic sequences of the amorphous phase, a higher temperature mode α at 70 °C assigned with the dielectric manifestation of the glass transition and an intermediate mode labelled β at −10 °C. This last mode which is independent from particles size corresponds to the relaxation of water amide complexes. When the particles size decreases, a shift towards lower temperature of nearly 10° for the γ mode and 6° for the α mode, is reported. Then, $BaTiO_3$ particles play the role of a plasticizer for the amorphous phase of the matrix.

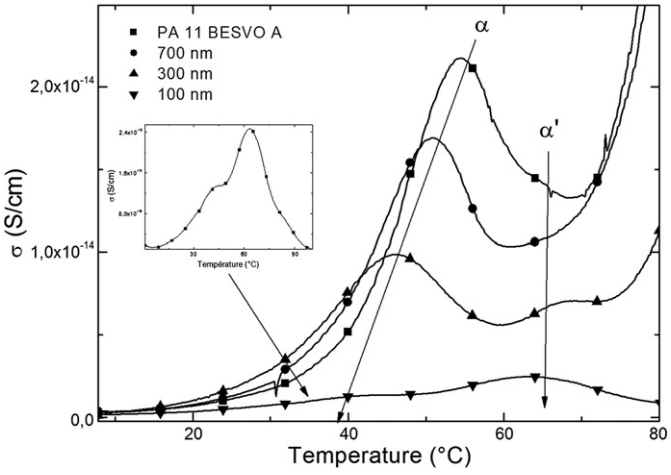

Fig. 6. TSC thermograms normalized to the volume fraction of organic phase of (■) polyamide 11 and PA 11/$BaTiO_3$ composites with $\phi = 12\%$ and particles size of (●) 700 nm, (▲) 300 nm and (▼) 100 nm.

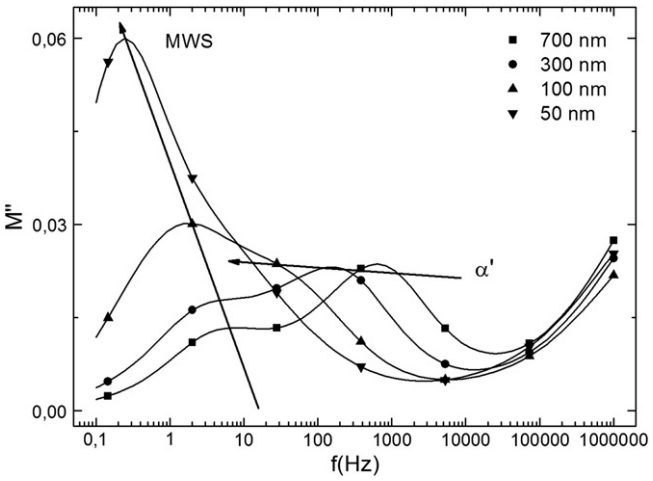

Fig. 7. Frequency dependence of the dielectric loss M″ (T = 100 °C) of PA 11/ $BaTiO_3$ composites with $\phi = 12\%$ and particles size of (■) 700 nm, (●) 300 nm, (▲) 100 nm and (▼) 50 nm.

In order to quantify the influence of the $BaTiO_3$ particles size on the γ and α molecular mobility, the Havriliak–Negami equation [21] has been fitted to the dielectric permittivity data. In the frequency range of 0.1 Hz − 1 MHz, the temperature dependence of the γ relaxation is

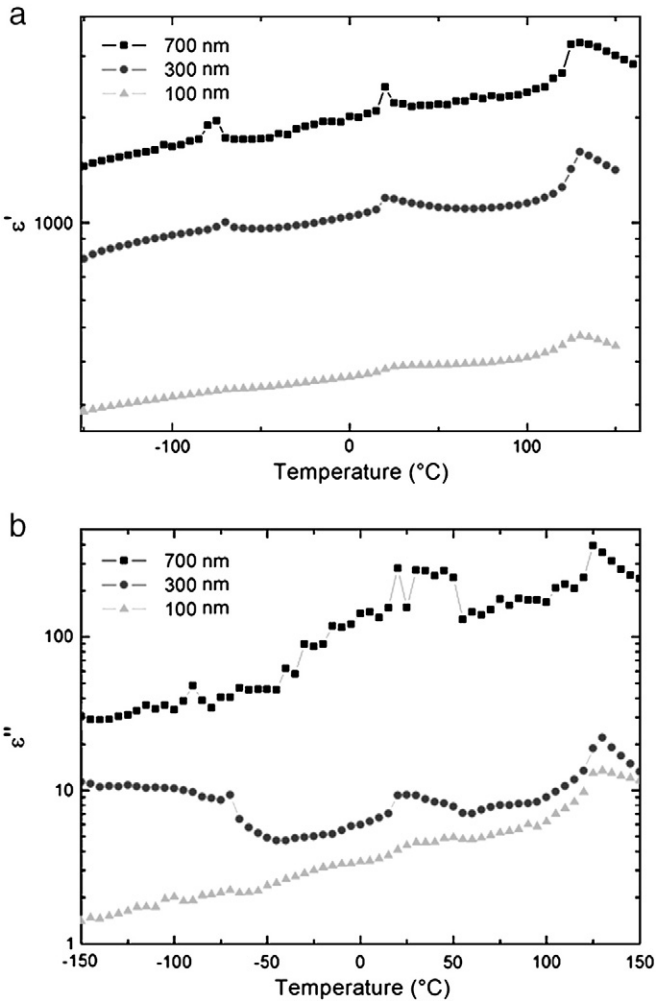

Fig. 8. Temperature dependence of (a) ε′ and (b) ε″ (f = 1 kHz) of $BaTiO_3$ ceramics sintered by Spark Plasma Sintering from nanoparticles of (■) 700 nm, (●) 300 nm, (▲) 100 nm.

ranging from −90 °C to −50 °C with the Arrhenius behaviour independent from the particles size. At fixed temperature, relaxation times decrease. The α modes fitted in the temperature range from 60 °C to 90 °C have a Vogel-Tammann-Fulcher temperature dependence. The relaxation times evolution is similar to the one of the γ mode. If the particles size decreases, the molecular dynamics of α relaxation is shifted towards lower relaxation times. The parameters of γ and α modes extracted from Arrhenius and VTF equations have been reported in Table 1. The activation energy Ea of the γ relaxation decreases with the filler size from 46 kJ mol^{-1} for 700 nm particles to 39 kJ mol^{-1} for 50 nm whereas τ_0 increases nearly by one decade.

For the α mode, τ_0 decreases with the particles size from 6.10^{-12} s for 700 nm to 6.10^{-17} s for 50 nm particles. In a same way, the α_f parameter associated with the free volume decreases by one decade. The fragility index $D = 1/(\alpha_f T_0)$ increases with the decrease of the filler diameter. D is maximal for 100 nm composites. The fragility index evolution is coherent with the evolution of the hydrogen bond density in the liquid phase of the matrix.

3.2. Dielectric relaxation modes in thermal analysis

The thermo stimulated current technique allows us to follow the evolution of relaxations modes as a function of nanofiller size. The influence of $BaTiO_3$ on the α molecular mobility has been studied. All the depolarization current thermograms I were normalized to the volume fraction of PA 11, the sample area S and the applied static electric field E following the Eq. 2:

$$\sigma = I / \{E \cdot S(1-\phi)\} \quad (2)$$

In the high temperature range, two relaxations are pointed out: α the lower temperature one and α′ the higher temperature one. The α mode is associated with the dielectric manifestation of the glass transition. The molecular origin of the α′ relaxation will be discussed in the next section.

The particles size influence on the high temperature TSC relaxations is shown in Fig. 6. The $BaTiO_3$ volume fraction is maintained at 12%. The TSC thermogram of the PA 11 matrix is reported as reference. For PA 11 and PA 11/$BaTiO_3$ 700 nm composites, only one relaxation mode at 50 °C is distinguishable. This α process is attributed to the dielectric manifestation of the glass transition of the free amorphous phase. For lower particles size, a higher temperature mode α′ is recorded. As previously reported, for PA11/$BaTiO_3$ 300 nm with $\phi = 12\%$, the α process is more important than the α′ one. For lower size particles, the α′ process is predominant. $T_{\alpha'}$ increases by 10° and the amplitude by 1 decade upon decreasing of particles size. This evolution is coherent with the assignment of α′ with a relaxation in the constrained amorphous phase.

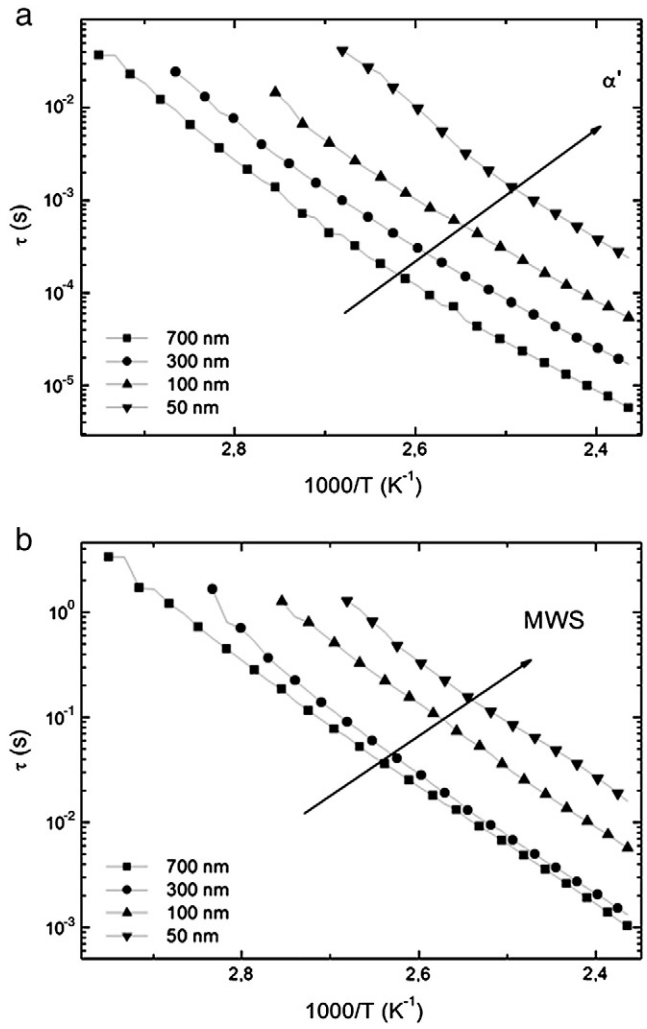

Fig. 9. Arrhenius plot of the relaxation times τ_{HN} of (a) α′ and (b) MWS relaxations of PA 11/$BaTiO_3$ composites with $\phi = 12\%$ and particles size of (■) 700 nm, (●) 300 nm, (▲) 100 nm and (▼) 50 nm extracted from Havriliak–Negami's modulus equation.

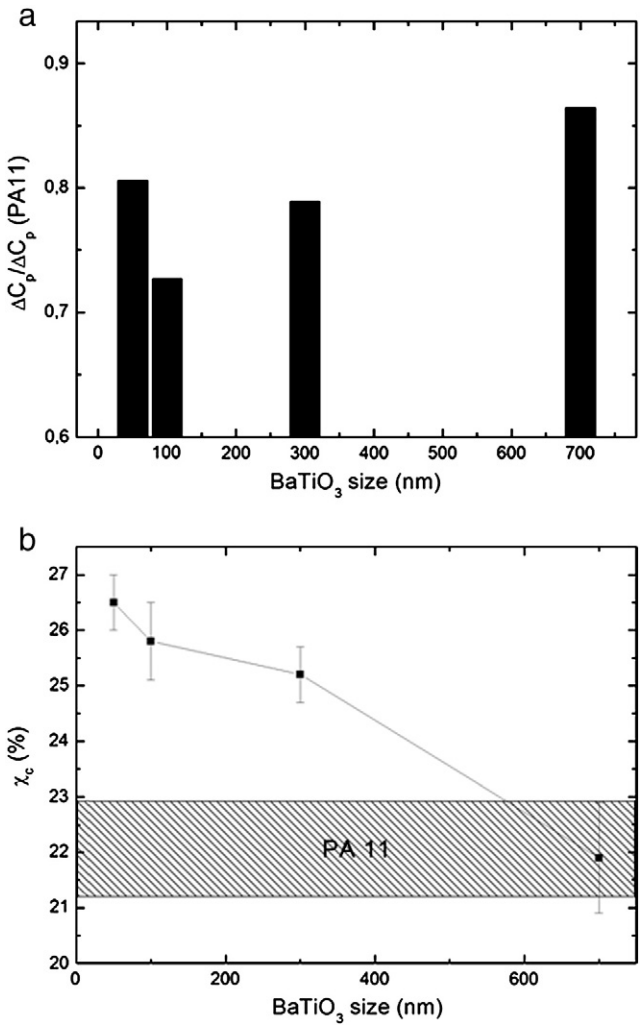

Fig. 10. Differential scanning calorimetric (DSC) measurements of (a) ΔCp normalized to ΔCp of polyamide 11 associated with the glass transition and (b) crystalline degree of PA 11/$BaTiO_3$ composites with $\phi = 12\%$ versus nanoparticles size.

4. Discussion

4.1. Dielectric relaxations in the liquid state

In order to analyze the particles size influence on the relaxations occurring above T_g, the dielectric modulus M^* formalism is required. The dielectric loss modulus M'' versus frequency is reported in Fig. 7, at 100 °C, for the different particles sizes. For PA 11/$BaTiO_3$ composites with $\phi = 12\%$, two relaxation modes are pointed out. The high frequency relaxation noted α' is attributed to the dielectric manifestation of the constrained amorphous phase. The presence of heterogeneities implies Maxwell–Wagner–Sillars polarization. The low frequency contribution has been labelled MWS mode. Nevertheless an ohmic contribution might interfere with this phenomenon. α' and MWS modes are shifted toward lower frequencies upon decreasing of particles size. The α' relaxation strength is invariant while the MWS relaxation strength increases upon decreasing of the particles size. The increase of M'' is mainly due to the ε' decreasing (cf Eq. 1) at high temperature and low frequency.

In order to check the origin of the decrease of ε' and ε'' with the particles size, $BaTiO_3$ particles have been elaborated by Spark Plasma Sintering (SPS). This technique allows us to obtain bulk ceramics with restrained grain growth. Dielectric response of bulk ceramics elaborated with 700 nm to 100 nm particles is shown in Fig. 8. A slight decrease of ε' and ε'' values upon increasing of ceramic grains size is shown. This decrease is not visible below T_g due to the high difference between $BaTiO_3$ and PA permittivity values. Above T_g, due to the increase of ε' associated with MWS phenomenon, the real and imaginary parts of dielectric permittivity of the inorganic and organic phases are closer and the influence of $BaTiO_3$ particles permittivity is visible.

The dynamics of the α' and MWS relaxations have been deduced from the fitting of M'' with the Havriliak–Negami equation in the modulus formalism. The Arrhenius plot of the relaxation times is shown in Fig. 9. The α' relaxation is VTF like. As the particles size decreases, this relaxation mode moves toward higher temperature. The MWS phenomenon has an Arrhenius behaviour. According to α', the MWS mode is shifted towards higher temperature for decreasing particles size. Its activation energy E_a decreases from 126 kJ mol^{-1} to 98 kJ mol^{-1} when particles diameter evolves from 700 nm to 50 nm. The associated pre-exponential factor τ_0 increases by 4 decades in the same particles size. As the MWS phenomenon is due to free carriers trapping at the interface between inorganic and organic phases over T_g[19], this dielectric contribution is dependent from the conductivity of the composite. As the composite become more insulating with the decrease of particles size, the MWS phenomenon takes longer times to establish.

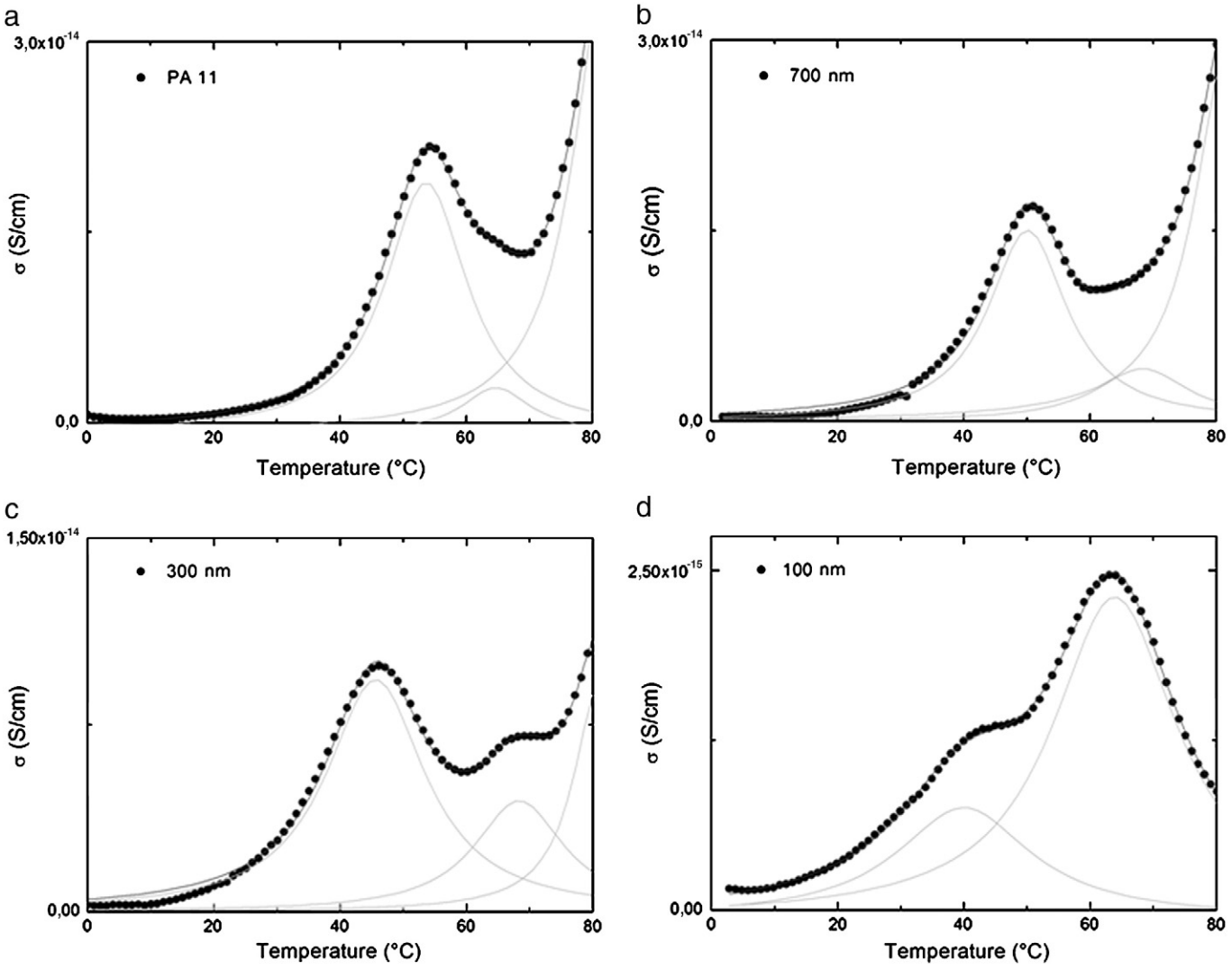

Fig. 11. (●) TSC thermograms normalized to the polymer volume fraction and Gaussian fits of (a) polyamide 11 and PA 11/$BaTiO_3$ composites with $\phi = 12\%$ and particles size (b) 700 nm, (c) 300 nm and (d) 100 nm.

4.2. Soft and rigid amorphous phases

The ΔCp step extracted from DSC as function of particles size is reported in Fig. 10a. A decrease of ΔCp with the particles diameter is pointed out; it is in good agreement with the TSC data showing also a decrease of the magnitude of the α relaxation associated with the soft amorphous phase The crystallinity ratio χ_c calculated from the DSC thermograms is reported in Fig. 10b. A 4% increase of χ_c is shown when the particles size decreases. This weak evolution of χ_c could not explain the concomitant 30% decrease of ΔCp. The hypothesis of a rigid amorphous phase that does not give a response either by DSC or by TSC around T_g is proposed. This phase would be favoured by small $BaTiO_3$ particles inducing local order stabilized by hydrogen bonds.

For the α and α′ modes, the TSC thermograms of hybrid composites have been fitted with Gaussian distributions in order to quantify the particles size influence on the current and they are reported in Fig. 11. For PA 11 and 700 nm hybrid composites, the α′ process is hidden by the conductivity contribution that appears at high temperature. For lower particles size, α and α′ are distinguished. The α′ peak temperature is maintained constant with the particles size. The experimental data fit allows us to extract the current evolution between α (σ_α) and α′ ($\sigma_{\alpha'}$) modes. The ratio $\sigma_\alpha/\sigma_{\alpha'}$ versus the particles size is reported in Fig. 12. This ratio linearly increases with the particles size logarithm. According to this fit, the ratio $\sigma_\alpha/\sigma_{\alpha'}$ of polyamide is reached for 4 μm. It is interesting to note that this value is close to the crystallite size of semi-crystalline polymers. The structural evolution defined by the ratio between the soft and rigid amorphous phase explains the fragile mechanical behaviour of the nanocomposites usually reported [18]: i.e. the more important the rigid phase is, the more fragile the composite.

For hybrid composites, the α′ relaxation is attributed to the molecular mobility of the constrained amorphous phase. This assumption is consistent with the fact that T_g measured by DSC is constant and it is coherent with the evolution of the α and α′ relaxations measured by TSC. At constant volume fraction when the particles size decreases, the organic/inorganic interface increases. By analogy with crystallites, this interface favours local order stabilized by hydrogen bonds. Then it results in an increase of the rigid amorphous phase.

5. Conclusion

The present study describes the influence of nanofiller size on the physical properties of the polymeric matrix of Polyamide 11/barium titanate ferroelectric nanocomposites. Above the glass transition temperature, dynamic dielectric spectroscopy allows us to follow the influence of particles size on relaxation modes. The Maxwell–Wagner–Sillars mode associated with heterogeneities and the mode associated with the glass transition are both shifted towards lower frequency when the $BaTiO_3$ particles size decreases.

Differential scanning calorimetry and thermally stimulated currents measurements show a decrease of the soft amorphous phase in the polymeric matrix upon decreasing of the nanofiller size. Simultaneously, the percentage of rigid amorphous phase is increasing. Smaller $BaTiO_3$ particles favour local ordering stabilized by hydrogen bonds.

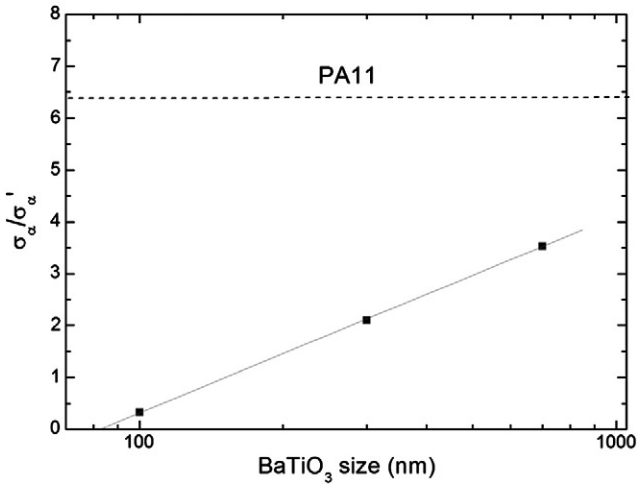

Fig. 12. Ratio between amplitude of α and α′ relaxations extracted from Gaussian fits of TSC thermograms of PA11/$BaTiO_3$ composites with $\phi = 12\%$ versus particles size.

Acknowledgements

The authors acknowledge the financial support of DGCIS and Région Midi-Pyrénées under NACOMAT program.

References

[1] H. Kawai, Japanese Journal of Applied Physics 8 (1969) 975.
[2] A.J. Lovinger, Science 220 (1983) 1115.
[3] M. Oshiki, E. Fukada, Journal of Materials Science 10 (1975) 1.
[4] L. Ibos, A. Bernes, C. Lacabanne, Ferroelectrics 320 (2005) 48.
[5] R.J. Klein, J. Runt, Q.M. Zhang, Macromolecules 36 (2003) 7220.
[6] H.M. Bao, J.F. Song, J. Zhang, Q.D. Shen, C.Z. Yang, Q.M. Zhang, Macromolecules 40 (2007) 2371.
[7] S.W. Or, H.L.W. Chan, C.L. Choy, Sensors and Actuators 80 (2000) 237.
[8] G.A. Samara, F. Bauer, Ferroelectrics 135 (1992) 385.
[9] J.I. Scheinbeim, J.W. Lee, B.A. Newman, Macromolecules 25 (1992) 3529.
[10] B. Hilczer, J. Kułek, E. Markiewicz, M. Kosec, B. Mali, Journal of Non-Crystalline Solids 305 (2002) 167.
[11] T.A. Perls, T.J. Diesel, D.W. Dobrov, Journal of Applied Physics 29 (1958) 1297.
[12] W.R. Cook, D.A. Berlincourt, Scholz, F.J, Journal of Applied Physics 34 (1963) 1392.
[13] R.E. Newnham, D.P. Skinner, L.E. Cross, Material Research Bulletin 13 (1978) 525.
[14] K.A. Hanner, A. Safari, R.E. Newnham, Runt, J Ferroelectrics 100 (1989) 255.
[15] T. Furukawa, K. Fujino, E. Fukada, Japonese Journal of Applied Physics 15 (1976) 2119.
[16] C.J. Dias, D.K. Das Gupta, IEEE Transactions on Dielectrics and Electrical Insulation 3 (1996) 706.
[17] J.F. Capsal, E. Dantras, L. Laffont, C. Lacabanne, Journal of Non-Crystalline Solids 356 (2010) 629.
[18] F. Fang, W. Yang, M.Z. Zhang, Z. Wang, Composites Science and Technology 69 (2009) 602.
[19] N.G. McCrum, B.E. Read, G. Williams, Anelastic and dielectric effects in polymeric solids, John Wiley & sons, New-York, 1967.
[20] F. Kremer, A. Schönals, Broad band dielectric spectroscopy, Springer, Berlin, 2003.
[21] S. Havriliak, S. Negami, Polymer 8 (1967) 161.